

Analytical Fault Detection and Isolation Algorithms Based on Rotation Matrices for a Three Axis Stabilized Satellite

DOI 10.7305/automatika.2014.12.385
UDK 629.056.8: 681.514.09
IFAC 5.9; 1.1.8

Original scientific paper

This paper presents fault detection and isolation (FDI) algorithms for attitude determination system (ADS) of a satellite including a sun sensor and a magnetometer. The suggested methodology is based on derivation of all possible rotations between reference and body frames and computation of Euler angles by them. Using the resulted Euler angles, some variance measures have been derived that offer a solution for analytical model-free fault detection mechanism. Consequently, when significant variations occur in these variances a fault occurrence is declared. It is shown that by properly categorizing the Euler angles computation methods, not only the faulty sensors but also their faulty components could be isolated. Based on the mentioned feature, four steps of fault isolation have been proposed. In the first step, fault occurrence in only one component of a sensor is isolated. In the second step, two faults in two different sensors are investigated. In the third step, two faults in one sensor are evaluated that means a high level of failure in the sensor. Finally, if fault does not belong to the above categories, it means that more than 50% damage has been occurred in the ADS hardware. Through extensive simulation studies, the desired performance and accuracy of the outlined methods have been demonstrated.

Key words: Attitude Determination System, Satellite, Sensors, Euler angles, Fault Detection, Fault Isolation.

Analiitička detekcija pogreške i izolacijski algoritmi zasnovani na rotacijskim matricama za satelit s tri osi. Ovaj rad prikazuje detekciju pogreške i izolacijske algoritme za sustav određivanja stanja satelita uključujući sunčani senzor i magnetometar. Predložena metodologija temelji se određivanju svih mogućih rotacija među referentnim i stvarnim koordinatnim sustavima i Eulerovim kutovima među njima. Koristeći Eulerove kutove dobivene su varijance pomoću kojih se dobiva rješenje za analitičku detekciju pogreške bez korištenja modela. U slučaju značajnih promjena varijance detektirana je pogreška. Pokazano je da se prikladnim kategoriziranjem izračuna Eulerovih kutova uz pogreške senzora može i izolirati komponenta senzora koja je uzrokovala pogreku. Na temelju toga predlažu se četiri koraka izolacije pogreške. U prvom koraku, izolirano je postojanje pogreške u samo jednom senzoru. U drugom koraku, istražuju se dvije pogreške u dva različita senzora. U trećem koraku, promatraju se dvije pogreške u jednom senzoru što će značiti visoku razinu pogreške u senzoru. Konačno, ukoliko pogreška ne pripada niti jednoj od navedenih kategorija, to znači da je prisutno oštećenje opreme veće od 50 %. Kroz opsežne simulacije prikazano je željeno ponašanje i točnost navedene metode.

Ključne riječi: sustav za određivanje stanja, satelit, senzori, Eulerovi kutovi, detekcija pogreške, izolacija pogreške

1 INTRODUCTION

Satellite pointing accuracy is one of the main requirements that its satisfaction depends on the perfect-healthy performance of the attitude determination and control system (ADCS). Investigation of fault events in different missions shows that many of occurred faults in the sensors and actuators have led to the degradation of expected services, loss of vehicle control or in case of total failures, catastrophic loss of mission [1]. Therefore, there is a need to develop fault tolerance tools in a safety critical system such

as ADCS, capable of detecting and isolating any component fault.

In this paper, the problems of fault detection and isolation for attitude determination sensors are addressed. Attitude determination (AD) is the process of computing the orientation of the satellite relative to a reference frame. To completely determine the orientation of a rigid body satellite, three angles between the satellite body frame and the selected reference frame must be specified.

These three angles are known as attitude angles or Eu-

ler angles. Consequently, the objective of AD in a satellite is to generate measurements of the attitude angles for use by its controllers. A procedure frequently used on three axis stabilized satellites is to determine the attitude by measuring the orientation of two reference vectors fixed in inertial space. In this paper, the above vectors are chosen as the sun vector and the earth magnetic field vector. The sun vector specifies at each time the satellite orientation with respect to the sun. Also, the magnetic field vector shows the earth magnetic field coordinates at each orbital position around the earth. So, a two axis sun sensor and a three axis orthogonal magnetometer have been selected as attitude determination hardware to provide the mentioned reference vectors in the body frame [2].

Today, analytical model based fault detection and isolation methods have been applied in the ADS as a mature and structured field of research. Most of these approaches are relied on residual generation by the Kalman filters, using the Eigen structure assignment techniques or sensor fault estimation by different types of observers [3, 4]. In [5], two Kalman filters have been used for fault detection and isolation based on measured outputs from gyros, sun sensor and magnetometer. Also, the problem of fault detection and isolation for satellite nonlinear dynamics has been addressed using the Extended Kalman Filter (EKF) and the Unscented Kalman Filter (UKF) [6]. The authors of [7] have suggested a robust UKF that provides a more effective convergence of the state estimation error. Another application of unscented Kalman filters, entitled federated UKF, has been presented in [8]. This approach that uses a local UKF for each of sensors provides the fault detection, fault isolation and continuity of the estimation process. Eigen structure assignment techniques propose another alternative for fault detection based on residual generation. In [9], an Eigen structure assignment technique has been used for fault detection of gyros in the Indian satellite named IRS. Residual generation in this approach can be accomplished such that the fault isolation between different sensors becomes possible. Another category of FDI mechanisms are observer based methods. In this regard, [10] has been proposed predictive filters for sensor fault reconstruction. Adaptive methods are other fault estimation techniques. For instance, the methodology suggested by [11, 12] uses neural networks in combination with adaptive techniques to estimate the fault magnitude. Sliding mode observers have also a similar operational technique in which the equivalent output injection signal is utilized for fault reconstruction purposes [13-16].

All the fault detection and isolation mechanisms detailed above, are model based approaches which operate based on satisfaction of sensors and actuators outputs with respect to the expected dynamical relations of system. The above principle, despite proposing the mentioned advan-

tages, loses its ability in conditions that simultaneous faults occur in both sensors and actuators. To deal with the above problem i.e. removing the mentioned restrictive assumption, this paper presents a novel analytical model-free method that provides the FDI features in the ADS independent of the health status of actuators. This approach is obtained based on all possible rotations between reference and body frames and computation of Euler angles by them. Using the resulted Euler angles, some variance measures are derived that offer a solution for analytical model-free fault detection mechanism. Therefore, when significant variations occur in these variances, it is argued that the measurement noises alone cannot explain these variations and so our proposed algorithm declares a fault happening.

After fault detection, the faulty sensors should be determined in the isolation stage. In this paper, it is shown that by properly categorizing the computation methods, not only the faulty sensors but also their faulty components are isolated. Accordingly, four isolation steps are designed to determine the fault type. In the developed algorithm, these steps are checked sequentially and in each step the required warnings are declared. In the first step, fault occurrence in only one of the sensors components is evaluated. In the second step, two faults in two different sensors are investigated. In the third step, two faults in two components of a sensor are evaluated that warns a high level of failure in that sensor. Naturally, if fault does not belong to any of the above categories, at least three components of sensors have been deteriorated. In this condition, an indicator flag is triggered to warn a more than 50% failure in the ADS hardware.

As it was mentioned, the suggested solution proposes model-free fault detection and isolation mechanisms which their performances are independent of the attitude control system health. So, fault detection and isolation in the ADS can be achieved even when the actuators are faulty. Moreover, the cited method suggests an analytical approach; so, a higher reliability is achieved by avoiding additional mass, power and cost.

The outline of this paper is as follows. In section 2, defined coordinate systems are described. Derivation stages of the Euler angles based on all possible rotations are stated in section 3. Design of fault detection algorithm is introduced in section 4. In section 5, fault isolation algorithms are presented. Numerical simulations for a number of faulty scenarios that occur in the attitude sensors are included in section 6. Finally, conclusions are presented in section 7.

2 DEFINED COORDINATE SYSTEMS

As mentioned before, the attitude angles describe the relation between the satellite body coordinate system and

a reference frame. Since in this paper, the satellite motion is assumed in an orbit around the earth, the orbital frame is selected as the reference frame. The above coordinate frames which have been used for the satellite motion analysis are defined as follows; 1 orbital frame which has its origin at the satellite's center of mass, Z_o axis points toward the center of mass of the earth, X_o axis is perpendicular to the Z_o axis in the direction of the satellite velocity and Y_o axis completes a three-axis right-handed orthogonal system, 2 body fixed frame which has its origin at the satellite's center of mass and its axes (X_b, Y_b and Z_b) aligned with the principal axes of satellite inertia.

3 EULER ANGLES DERIVATION FROM THE ROTATION MATRICES

As mentioned in the previous section, the Euler angles define how the satellite body frame is related to the orbital frame (as reference frame). This rotation is described using a rotation matrix that maps vectors from the orbital frame to the body frame. This matrix is expressed in triangular functions of the Euler angles. In our treatment, the Euler angles are defined as the rotation angles about the body axes as follows: φ about the X axis, θ about the Y axis and ψ about the Z axis.

According to different order of rotation of the axes of the satellite with respect to the reference frame, there may be as many as rotation matrices. A well-known rotation matrix which has been widely used in the aerospace applications is obtained by respectively doing the rotations of ψ about the Z axis, θ about the Y axis and φ about the X axis (Figure 1). So, the b_oT transformation matrix is computed by doing the following matrix multiplications:

$${}^b_oT = T_\psi \cdot T_\theta \cdot T_\varphi = \begin{bmatrix} c\theta c\psi & c\theta s\psi & -s\theta \\ s\phi s\theta c\psi - c\phi s\psi & s\phi s\theta s\psi + c\phi c\psi & s\phi c\theta \\ c\phi s\theta c\psi + s\phi s\psi & c\phi s\theta s\psi - s\phi c\psi & c\phi c\theta \end{bmatrix}, \tag{1}$$

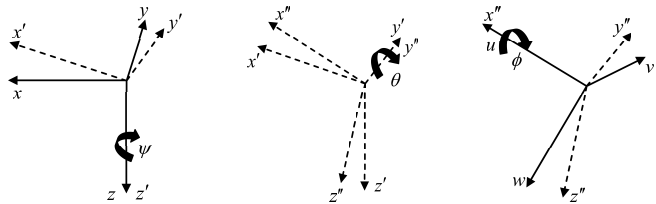
where c and s denote \cos and \sin , respectively. We refer the reader to [17] to see components of the T_ψ , T_θ and T_φ matrices. The attitude determination system derives the above transformation matrix using the sensor measurements; accordingly, the Euler angles (the ADS outputs) are computed as follows using the b_oT components:

$$\theta = -\arcsin(T_{13}), \tag{2}$$

$$\phi = \arctan(T_{23}/T_{33}) \tag{3}$$

$$\psi = \arctan(T_{12}/T_{11}) \tag{4}$$

Calculating Euler angles using the rotation matrix method is simplified if the sun vector and the magnetic vector are in the form $[0 \ 0 \ 1]^T$ and $[b_1 \ 0 \ b_3]^T$ respectively where b_1 and b_3 are arbitrary parameters (these calculations will be detailed in the next sections). Since in the satellite systems, the orbital frame is chosen as the reference frame, all above six components are nonzero. To resolve this problem, an intermediate frame is derived in this paper where the mentioned reference vectors are expressed in the desired form. This coordinate system is obtained by applying sequential transformations on the orbital frame.



Slika 1. Relation between the axes and the rotation angles

So, in the design procedure of the FDI mechanisms, the orbital frame should be replaced by the intermediate frame and all the rotation matrices and the Euler angles should be derived relative to this frame. To avoid confusion, in the rest of this paper these angles are called the "intermediate Euler angles $\varphi_v, \theta_v, \psi_v$ ". It is important to note that the proposed FDI mechanisms use the intermediate Euler angles and are independent of the AD algorithm. In the following, the intermediate frame is defined in section 3.1 and then in section 3.2, computation methods of the Euler angles based on the mentioned intermediate frame are stated.

3.1 Definition of the intermediate frame

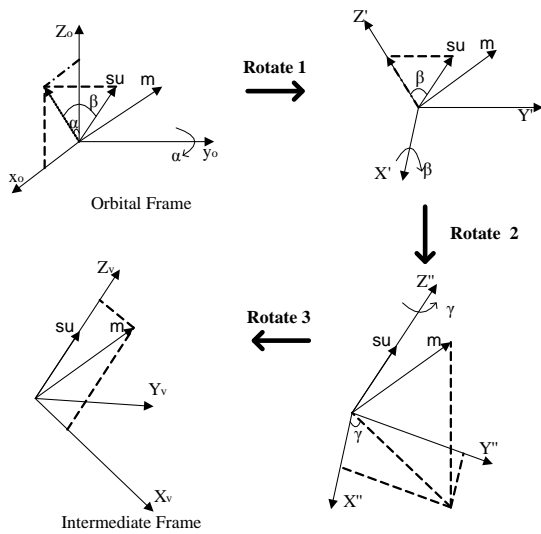
Intermediate frame is defined such that the sun vector su and the earth magnetic vector m in this frame are stated as follows:

$$su_v = [0 \ 0 \ 1]^T, m_v = [b_1 \ b_2 \ b_3]^T. \tag{5}$$

Figure 2 illustrates the intermediate frame and the above attitude vectors. As shown in this figure, Z_v axis is corresponding to the sun vector su , X_v axis is selected such that the magnetic vector is placed on the X_v - Z_v plane and Y_v axis completes a three-axis right-handed orthogonal system. The orbital frame, defined in section 2, has been shown in this figure. The sun vector and the earth magnetic vector in the orbital frame are denoted respectively as $[su_{x_o} \ su_{y_o} \ su_{z_o}]^T$ and $[m_{x_o} \ m_{y_o} \ m_{z_o}]^T$.

The sun vector in the orbital frame is derived by modelling the relative position of the satellite and the sun. Also, the earth magnetic vector is computed using the International Geomagnetic Reference Field (IGRF) earth magnetic model [2].

Therefore, the mentioned vectors are model vectors that are always known. After transformation into the intermediate frame, the resulted vectors su_v and m_v are also known (i.e. b_1 and b_3 in (5) are known). According to the defined intermediate frame, the transformation matrix between the orbital and body frames, is determined as:



Slika 2. Required rotations for obtaining the intermediate frame

$${}^b_oT = {}^b_vT \times {}^v_oT, \tag{6}$$

where b_vT is the transformation matrix between the intermediate and body frames and v_oT is the transformation matrix between the orbital and intermediate frames.

In the above equation, v_oT is a known matrix that obtained using the modelled vectors in the orbital frame. This matrix can be derived by application the following rotations on the orbital frame and using the sun vector and the magnetic vector modelled in this frame:

1) Rotation about the Y_o axis with angle α which is the angle between the sun vector projection on the X_o-Z_o plane and the Z_o axis (Figure 2). This angle is obtained as below:

$$\alpha = \tan^{-1}(su_{x_o}/su_{z_o}), \tag{7}$$

2) Rotation about the X axis of the rotated frame with angle β which is the angle between the sun vector projection on the X_o-Z_o plane and the sun vector (Figure 2). This angle is computed as:

$$\beta = \tan^{-1}(su_{y_o}/\sqrt{su_{x_o}^2 + su_{z_o}^2}), \tag{8}$$

By application of the above rotations, the sun vector is transformed to $su = [0 \ 0 \ 1]^T$ and the magnetic vector is transformed to $m = [m'_1 \ m'_2 \ m'_3]^T$.

3) Rotation about the Z axis of the rotated frame with angle γ which is the angle between the magnetic vector projection on the $X-Y$ plane and the X axis (Figure 2). This angle is calculated as:

$$\gamma = \tan^{-1}(m'_2/m'_1), \tag{9}$$

Accordingly, v_oT is derived as:

$${}^v_oT = \begin{bmatrix} 1 & 0 & 0 \\ 0 & c\beta & -s\beta \\ 0 & s\beta & c\beta \end{bmatrix} \times \begin{bmatrix} c\alpha & 0 & -s\alpha \\ 0 & 1 & 0 \\ s\alpha & 0 & c\alpha \end{bmatrix} \times \begin{bmatrix} c\gamma & s\gamma & 0 \\ -s\gamma & c\gamma & 0 \\ 0 & 0 & 1 \end{bmatrix} = \begin{bmatrix} cac\gamma & cas\gamma & -sa \\ -s\gamma c\beta - s\beta sac\gamma & c\gamma c\beta - s\beta sas\gamma & -s\beta ca \\ -s\gamma s\beta + c\beta sac\gamma & c\gamma s\beta + c\beta sac\gamma & c\beta ca \end{bmatrix} \tag{10}$$

The b_vT matrix in 6 is an important transformation that is associated with the sensors measurements as follows:

$$\begin{bmatrix} su_x \\ su_y \\ su_z \end{bmatrix} = {}^b_vT \times \begin{bmatrix} 0 \\ 0 \\ 1 \end{bmatrix}, \tag{11}$$

$$\begin{bmatrix} m_x \\ m_y \\ m_z \end{bmatrix} = {}^b_vT \times \begin{bmatrix} b_1 \\ 0 \\ b_3 \end{bmatrix}, \tag{12}$$

where $[m_x \ m_y \ m_z]^T$ and $[su_x \ su_y \ su_z]^T$ are respectively the outputs measured by the magnetometer and the sun sensor in the body frame. So, fault occurrence in the sensors will affect the matrix components. In the next section, we focus on this transformation and derive different calculation methods of this matrix. Also, different computation methods of the intermediate Euler angles using the above matrix components are described. These angles are used to design the FDI mechanisms.

3.2 Derivation of the rotation matrices between the intermediate and body frames

As it was mentioned, before designing the fault detection and isolation algorithms, it is necessary to derive all possible rotation matrices between the intermediate and body frames. For this, first, the yaw-pitch-roll (YPR) rotation matrix that is a common rotation in aerospace applications is considered. Then, based on this rotation, all possible computation methods to determine the intermediate Euler angles are derived. Afterwards, other rotation sequence formulations for calculating the intermediate Euler angles are calculated.

The rotation matrix YPR that is generated by respectively the rotations ψ_v about the Z axis, θ_v about the Y axis and φ_v about the X axis is given by:

$${}^bT_{YPR} = \begin{bmatrix} c\theta_v c\psi_v & c\theta_v s\psi_v & -s\theta_v \\ s\varphi_v s\theta_v c\psi_v - c\varphi_v s\psi_v & s\varphi_v s\theta_v s\psi_v + c\varphi_v c\psi_v & s\varphi_v c\theta_v \\ c\varphi_v s\theta_v c\psi_v + s\varphi_v s\psi_v & c\varphi_v s\theta_v s\psi_v - s\varphi_v c\psi_v & c\varphi_v c\theta_v \end{bmatrix} \quad (13)$$

So, according to 11, 12 and 13, the intermediate Euler angles are computed as follows:

$$\begin{aligned} \theta_v &= -\sin^{-1}(su_x) \\ \phi_v &= \sin^{-1}(su_y / \cos \theta_v) \\ \psi_v &= \cos^{-1}([m_x + b_1 \sin \theta_v] / b_3 \cos \theta_v) \end{aligned}, \quad (14)$$

As it can be observed, the intermediate Euler angles can be determined when some components of the attitude sensors are not available. For instance in 14, only the su_x , su_y and m_x components are required for rotation angles derivation. The above computation method is titled YPR1. Once again, using another combination of components in the rotation matrix YPR (see again (11), 12 and 13) the intermediate Euler angles can be computed according to:

$$\begin{aligned} \varphi_v &= \tan^{-1}(su_y / su_z) \\ \theta_v &= \cos^{-1}(su_y / \sin \varphi_v) \\ \psi_v &= \cos^{-1}([m_x + b_1 \sin \theta_v] / b_3 \cos \theta_v) \end{aligned}, \quad (15)$$

In this case, the three components su_z , su_y and m_x are used to determine the intermediate angles. This computation method is titled YPR2. Similarly, the rotation angles can be obtained using four another approaches which use some subsets of sensors output components. The corresponding computation methods are not presented here for brevity.

In the following, the procedure used for another 11 rotations is explained. These rotations with consideration

of their sequences are denoted as YPY, YRY, RPR, RYR, PRP, PYP, RYP, PRY, RPY, YRP and PYR which R stands for roll rotation, Y stands for yaw rotation and P stands for pitch rotation. Each of these rotations leads to different computation methods which based on, the intermediate Euler angles are determined. For instance, the rotation RPY that is computed using the rotations φ_1 about the X axis, θ_1 about the Y axis and ψ_1 about the Z axis, will be stated as:

$${}^bT_{RPY} = \begin{bmatrix} c\theta_1 c\psi_1 & c\varphi_1 s\psi_1 + s\varphi_1 s\theta_1 c\psi_1 & s\varphi_1 s\psi_1 - c\varphi_1 s\theta_1 c\psi_1 \\ -c\theta_1 s\psi_1 & c\varphi_1 c\psi_1 - s\varphi_1 s\theta_1 s\psi_1 & s\varphi_1 c\psi_1 + c\varphi_1 s\theta_1 s\psi_1 \\ -s\theta_1 & -s\varphi_1 c\theta_1 & c\varphi_1 c\theta_1 \end{bmatrix}, \quad (16)$$

According to 11, 12 and 16, the rotation angles φ_1 , θ_1 and ψ_1 can be obtained as below in which the components m_x , m_y , m_z and su_z are used:

$$\begin{aligned} \theta_1 &= -\sin^{-1}((m_z - b_3 su_z) / b_1) \\ \varphi_1 &= \cos^{-1}(su_z / \cos \theta_1) \\ \psi_1 &= \sin^{-1}((Bm_x - Am_y) / (A^2 + B^2)) \end{aligned}, \quad (17)$$

where

$$\begin{aligned} A &= b_3 \cos \theta_1 - b_1 \sin \theta_1 \cos \varphi_1 \\ B &= b_3 \sin \varphi_1 \end{aligned}. \quad (18)$$

The above computation method is titled RPY1. An important point to note is that intermediate Euler angles are defined according to the aerospace sequence. If a different rotation sequence is used, the rotation angles obtained are different from the standard intermediate Euler angles. So, the angles obtained have to be converted to the standard Euler angles. The rotation angles φ_1 , θ_1 and ψ_1 derived from 17 are converted to the standard Euler angles using 19 below:

$${}^bT_{RPY} = {}^bT_{YPR}, \quad (19)$$

Using the above equality together with 13 and 16, the intermediate Euler angles can be derived as:

$$\begin{aligned} \theta_v &= \sin^{-1}(\cos \varphi_1 \sin \theta_1 \cos \psi_1 - \sin \varphi_1 \sin \psi_1) \\ \varphi_v &= \cos^{-1}(\cos \varphi_1 \cos \theta_1 / \cos \theta_v) \\ \psi_v &= \cos^{-1}(\cos \theta_1 \cos \psi_1 / \cos \theta_v) \end{aligned}, \quad (20)$$

In the RPY rotation, the rotation angles can also be computed using another sensors measurement data as:

$$\begin{aligned} \theta_1 &= \sin^{-1}((m_z - b_3 su_z) / b_1) \\ \varphi_1 &= \cos^{-1}(su_z / \cos \theta_1) \\ \psi_1 &= \sin^{-1}((Dsu_x - Csy) / (C^2 + D^2)) \end{aligned}, \quad (21)$$

where

$$\begin{aligned} C &= -\sin \theta_1 \cos \varphi_1 \\ D &= \sin \varphi_1 \end{aligned} \quad (22)$$

The above method is titled RPY2. Similar to the RPY1 method, the intermediate Euler angles can be computed according to 20. It can be demonstrated that the RPY rotation can only lead to the mentioned computation methods. After investigation of all 12 rotations and using different sensors components, similar to the procedure detailed above, it can be shown that the intermediate Euler angles can be obtained from 25 independent computation methods. Table 1 summarizes the YPR and RPY rotations and different sensors measurement data which are required for the mentioned methods. Other rotations are not included in this table because of space limitations.

4 FAULT DETECTION ALGORITHM

In this section, the fault detection algorithm using the derived computation methods is detailed. As mentioned before, after fault occurrence in each of the sensors components, the proposed computations methods are affected. This fact motivated us to introduce some variance measures using the intermediate Euler angles which have been resulted in by all of the 25 methods. These variances are defined as:

$$\sigma_{\varphi_v}^2 = \frac{\sum_{i=1}^{25} (\varphi_{v_i} - \bar{\varphi}_v)^2}{25}, \quad (23)$$

$$\sigma_{\theta_v}^2 = \frac{\sum_{i=1}^{25} (\theta_{v_i} - \bar{\theta}_v)^2}{25}, \quad (24)$$

$$\sigma_{\psi_v}^2 = \frac{\sum_{i=1}^{25} (\psi_{v_i} - \bar{\psi}_v)^2}{25}, \quad (25)$$

where φ_{v_i} , is the intermediate Euler angles resulted in by the i th method and $\bar{\varphi}_v$ is the mean value of φ_{v_i} variances.

Similar expressions can be derived for $\sigma_{\theta_v}^2$ and $\sigma_{\psi_v}^2$ variances. Accordingly, if the sun sensor and the magnetometer are not faulty, the intermediate Euler angles provided by all of the 25 methods are consistent to each other and hence the variances obtained by the above equations have a value near to zero. In fact, since the sensors outputs are corrupted by noises, the variances are not exactly zero and vary in a narrow bound around the zero. When a fault occurs in the sensors components, the methods that include the faulty components result in incorrect intermediate Euler angles. These incorrect angles lead to significant variations in the variances.

Tablica 1. Components contributed in each of the computation methods of the intermediate Euler angles

Rotation matrices	Number of methods	Attitude sensors components					
		Sun sensor			Magnetometer		
		su_x	su_y	su_z	m_x	m_y	m_z
YPR	1	✓	✓	×	✓	×	×
	2	×	✓	✓	×	✓	✓
	3	✓	×	✓	✓	×	×
	4	✓	✓	×	×	✓	✓
	5	✓	×	✓	×	✓	✓
	6	×	✓	✓	✓	×	×
RPY	7	×	×	✓	✓	✓	✓
	8	✓	✓	✓	×	×	✓
✓:	The computation method includes the related sensor component						
×:	The computation method does not include the related sensor component						

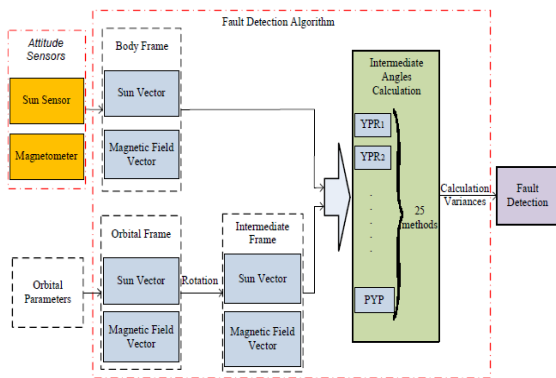
So, these variations can be used as a measure for fault detection. To prevent the noise effects, a threshold is selected for fault detection. The decision making process for fault detection is accomplished as follows:

$$\begin{aligned} IF \max(\sigma_{\varphi_v}^2, \sigma_{\theta_v}^2, \sigma_{\psi_v}^2) > threshold \\ \Rightarrow Fault \text{ Is Declared} \end{aligned} \quad (26)$$

Figure 3 depicts the interface details of the developed fault detection algorithm in the satellite onboard computer (OBC). For this, the sun sensor and the magnetometer measurements are received as inputs. Also, it is necessary that the sun vector and the magnetic field vector are generated in the orbital frame. After applying the rotation matrices, the above modeling vectors are transferred to the intermediate coordinate frame. So, according to the design presented in this section, it is possible to form the variance measures using the sensors measurements and the modelling vectors. These measures can realize the fault detection feature in the ADS sensors.

5 FAULT ISOLATION ALGORITHM

After fault detection, the faulty sensors should be isolated. In this section, it is shown that by suitable categorizing the computation methods derived in section 3, not only the faulty sensors but also their faulty components could be isolated. For this, four isolation steps have been developed. Figure 4 depicts the execution sequence of each of these four steps. The presented sequence is performed repeatedly in the ADS and the required warnings are declared.



Slika 3. The designed fault detection mechanism

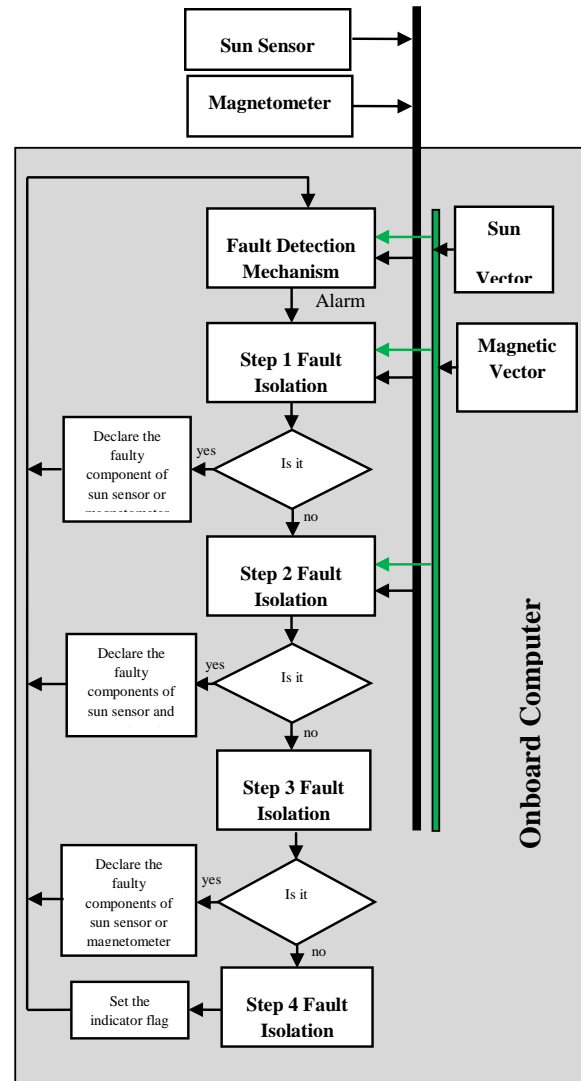
As it is illustrated in this figure, the developed fault detection and isolation algorithms are considered to implement in the satellite on-board computer (OBC) and receive as inputs the sensor measurements and modelling vectors.

- **Step 1:** Evaluation of fault occurrence in only one component of the sun sensor or one component of the magnetometer (type 1)
- **Step 2:** Investigation of simultaneous fault occurrence in one component of the sun sensor and one component of the magnetometer (type 2)
- **Step 3:** Evaluation of fault happening in two components of a sensor. This fault type warns a high level of failure in that sensor (type 3).
- **Step 4:** If fault does not belong to each of the above categories, a type 4 fault is declared. It means that at least three components of sensors have been deteriorated. In this case, the ADS is faced to more than 50% failure; so an indicator flag is assigned to show this event. Before describing each of the above steps, derived computation methods should be categorized so that the fault isolation can be provided.

If one of the sensors components is deteriorated due to fault occurrence (type 1 faults), the intermediate Euler angles in which the faulty component is not present, are not affected. For instance, a fault in the x component of the magnetometer affects the calculation of the intermediate Euler angles in the methods involving YPR1, YPR3, YPR6, RPY1, YRP3, YRP4, RYP2, PRY2, PYR1, PYR2, YPY2, RPR1, RYR1, PRP1 and PYP1, but the other methods remain unaffected.

Therefore, through utilizing the above idea, it is necessary to categorize the methods that don't include one of

the sensors components. Table 2 depicts such a categorization. According to this table, if a fault occurs in one of the sensors measurement data, only the intermediate Euler angles provided by the corresponding methods (depicted in the second column of the table) are correct and consistent to each other.



Slika 4. Different steps of the developed fault isolation mechanism

So, we should develop the variance parameters using the methods presented in Table 2. For instance, the $\sigma_{\varphi_{su_x}}^2$ variance corresponding to the x component of the sun sensor (see the first row of Table 2) is computed as follows:

$$\sigma_{\varphi_{su_x}}^2 = \frac{\sum \varphi_i (\varphi_i - \bar{\varphi}_{su_x})^2}{9}, \tag{27}$$

where φ_1 is substituted respectively by φ_{PYP} , φ_{PRP} ,

φ_{PRY2} , φ_{RYP2} , φ_{YRP4} , φ_{YRP1} , φ_{RPY1} , φ_{YPR6} , φ_{YPR2} and $\bar{\varphi}_{su_x}$ is calculated as follows:

Tablica 2. Categorizing the computation methods for type 1 faults

Faulty sensor components	Methods in which the component is not present
su_x	YPR2, YPR6, RPY1, YRP1, YRP4, RYP2, PRY2, PRP, PYP
su_y	YPR3, YPR5, RPY1, YRP2, YRP3, PRY2, PYR1, RPR, RYR
su_z	YPR1, YPR4, RYP2, PYR1, YPY1, YPY2, YRY, RPR, RYR, PRP, PYP
m_x	YPR2, YPR4, YPR5, RPY2, YRP1, YRP2, RYP1, PRY1, YPY1, YRY
m_y	YPR1, YPR3, YPR6, RPY2, YRP3, YRP4, PRY1, PYR2, YPY1, YRY
m_z	YPR1, YPR3, YPR6, YRP1, YRP2, RYP1, PYR2, YPY2

Tablica 3. Categorizing the computation methods for type 2 and type 3 faults

Row number	Faulty sensors components	Methods in which the components don't present
1	su_x-m_x	YPR2, YRP
2	su_x-m_y	YPR6, YRP4
3	su_x-m_z	YPR6, YRP
4	su_y-m_x	YPR5, YRP2
5	su_y-m_y	YPR3, YRP3
6	su_y-m_z	YPR3, YRP2
7	su_z-m_x	YPR4, YPY
8	su_z-m_y	YPR, YPY
9	su_z-m_z	YPR, YPY2
10	su_x-su_y	YPR2, YRP
11	su_x-su_z	YPR6, YRP4
12	su_y-su_z	YPR6, YRP
13	m_x-m_y	YPR5, YRP2
14	m_x-m_z	YPR3, YRP3
15	m_y-m_z	YPR3, YRP2

$$\bar{\varphi}_{su_x} = \frac{\sum \varphi_i}{9}. \tag{28}$$

Similar relations can be derived for $\sigma_{\theta_{su_x}}^2$ and $\sigma_{\psi_{su_x}}^2$ variances. In this paper, $\max(\sigma_{\phi_{su_x}}^2, \sigma_{\theta_{su_x}}^2, \sigma_{\psi_{su_x}}^2)$ is selected as a variance measure for x component of the sun sensor. Similar variance measures should be derived for other sensors data (su_y , su_z , m_x , m_y and m_z).

If one component of the sun sensor and one component of the magnetometer (type 2 faults) are deteriorated, we

need to search the computation methods in which the mentioned faulty components are not present. In other words, we require the methods that are not affected by the above faults. Fortunately, by investigation the computation methods, it can be shown that there is more than one computation method corresponding to each state of this fault type. Table 3 presents such a categorization for the mentioned fault happenings. In this case, similar to the procedure done for single fault occurrence, we should develop the variance measures using the existing methods in Table 3. In case that two faults occur in the magnetometer or two faults occur in the sun sensor (type 3 faults), similar computation methods can be found. These methods have been also presented in Table 3.

In the following sub sections, the mentioned isolation steps are detailed. As explained before, a fault of type 4 is declared if it does not belong to types 1, 2 and 3.

5.1 Step 1; fault isolation: fault occurrence in only one component of a sensor

According to Table 3, if fault occurs in only one of the sensors data, 5 variances from the total number of 15 variances don't change significantly, however other variances will have drastic variations. For example, if su_x is deteriorated due to fault occurrence, the presented variances in rows 1, 2, 3, 10 and 11 of Table 3 don't alter. With attention again to Table 3, it can be observed that if two components of sensors are subjected to fault, only one variance doesn't change significantly. For instance, after fault happening in su_y and m_x only the presented variance in row 4 of Table 3 doesn't change. In fact, the above observations give us a measure to distinguish between the states that one component is faced to a fault or two components are deteriorated. So, in step 1, we should first investigate the calculated variances in Table 3. If 5 variances have not varied significantly, it means that a type 1 fault has occurred.

Accordingly, after it is confirmed that a type 1 fault has occurred, we should investigate the calculated variances in Table 2 to determine the faulty component. The component corresponded to the variance that has the minimum value among all variances is the faulty component. For example in case that fault happens in su_x the variance computed in row 1 of Table 2, should have the minimum value. Note that if a fault of type 1 is diagnosed, it is not necessary to check other steps in the fault isolation chart.

5.2 Step 2; fault isolation: simultaneous fault occurrence in one component of the sun sensor and one component of the magnetometer

After investigation of calculated variances in Table 3, if it is observed that only one variance has not changed significantly (the minimum variance), two sensors data have

been subjected to fault. In this case, the components corresponded to this minimum variance (according to Table 3) are the faulty data. In this conditions, if this component belongs to rows 1 to 9 of Table 3, a type 2 fault is declared (two faulty components belong to different sensors), else, a type 3 fault has been happened that explained in the next section.

5.3 Step 3; fault isolation: fault occurrence in two components of a sensor

As mentioned in the previous section, after it is confirmed that two components are faulty, we should determine the components corresponding to the minimum variance. If, these components belong to rows 10 to 15 of Table 3, fault of type 3 is declared. It means that two faulty components belong to one sensor (sun sensor or magnetometer).

6 SIMULATION RESULTS

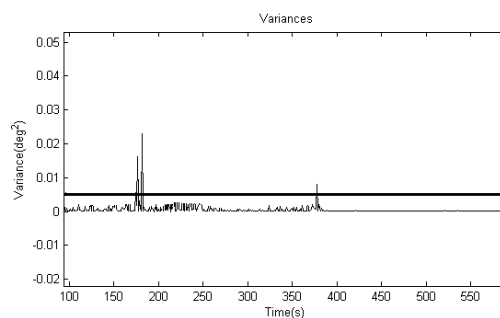
In this section, simulation results of the developed fault detection and isolation algorithms are presented to illustrate the performance of the mentioned algorithms. These simulations are carried out for a Low Earth Orbit (LEO) satellite with the altitude of 700 km, orbit inclination of 98° and right ascension of the ascending node of 4° . In the simulation model, output error of sensors is modelled as a white Gaussian noise. In this regard, the standard deviation of the magnetometer noise is selected as 50nT and the standard deviation of the sun sensor noise is chosen as 0.1° . The sampling rate of sensors is assumed to be equal to 1sec.

In the simulations, a threshold value of 0.004deg^2 has been selected for fault detection process. Figure 5 illustrates the mean value of variances in the absence of sensors faults. The variations of variances depicted in this figure are due to noisy measurements of sensors. As shown in this figure, the threshold value is chosen such that we can distinguish the fault effects from the effects caused by the sensors noises. Note that although in some special moments, the variances exceed the threshold value; however these mutations occur in a short time period less than 3 samples. Therefore, we have selected a 3 samples period for fault declaration. It is important to note that if the threshold value is chosen too small, it can be difficult to distinguish the fault effects from the effects caused by the sensors noises. Also, if the threshold value is selected conservatively, fault detection is done with a delay or the small faults may be not detected. After conducting several simulations, it has been concluded that we need 17 samples (in addition to the 3 samples required for fault detection) to follow the transient effects in the variances and select the minimum variance with confidence. In the performed

Tablica 4. The F_2 flag and its assigned values

Values	Fault type	Fault number	type
1	Fault occurrence in only one component of a sensor	Type 1	
2	Fault occurrence in one component of the sun sensor and one component of the magnetometer	Type 2	
3	Fault occurrence in two components of the sun sensor or two components of the magnetometer	Type 3	

simulations, F_1 , F_2 , F_3 and F_4 flags have been defined. F_1 has been assigned for fault declaration in the ADS and is valued by the fault



Slika 5. The threshold value and the mean value of variances in the absence of sensors faults

detection algorithm. F_2 has been assigned for fault isolation stage and is valued according to Table 4 to show the fault type. After determining the fault type, the faulty component/components of sensors should be specified. The flag F_3 has been assigned for this purpose and is valued according to Table 5 for different fault types. Finally, F_4 shows a type 4 fault occurrence. To investigate and study the performance of the designed algorithms, the following scenarios are considered.

Scenario 1: fault in the x component of the magnetometer

In this scenario, a bias fault with the magnitude 5000nT is introduced in the m_x at time $t = 200\text{s}$. Figure 6 shows that after fault occurrence, the minimum variance of the intermediate Euler angles (according to (26)) changes significantly that allows detecting the ADS fault. Therefore, F_1 is triggered after 3 samples. Now, the fault source should be isolated. Figure 7 depicts the calculated variances in

Table 3. This figure has been somewhat magnified to make it easier to compare the variance variations. According to this Figure, 5 variances (solid lines) have not changed significantly (they have small variations and are approximately zero) that means only one component is faulty (refer to section 5.1). Therefore, the value 1 is assigned to F_2 (Figure 8 (a)). To determine the faulty component, it is necessary to compute the variances in Table 2. Figure 9 shows these variances. As shown in this figure, the variance corresponding to m_x has

Tablica 5. The F_3 flag and its assigned values

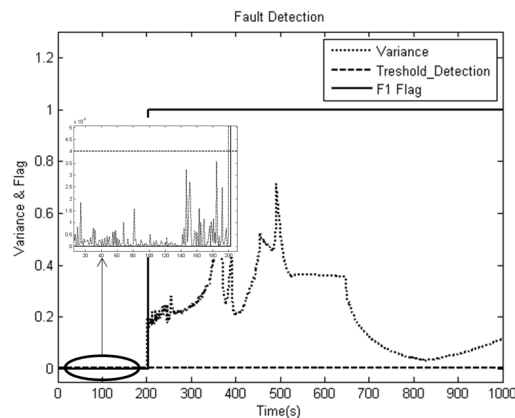
Fault type	Values	Corresponding affected components
1	1	su_x
	2	su_y
	3	su_z
	4	m_x
	5	m_y
	6	m_z
2	1	su_x-m_x
	2	su_x-m_y
	3	su_x-m_z
	4	su_y-m_x
	5	su_y-m_y
	6	su_y-m_z
	7	su_z-m_x
	8	su_z-m_y
	9	su_z-m_z
3	1	su_x-su_y
	2	su_x-su_z
	3	su_y-su_z
	4	m_x-m_y
	5	m_x-m_z
	6	m_y-m_z

the minimum value among all variances (it is approximately zero). So, the value 4 is assigned to F_3 to represent m_x as faulty component (Figure 8 (b)). Note that in this case, steps 2 and 3 are not necessary to execute. Also it takes totally 20 samples to detect the fault and isolate the faulty components (Figure 8(a)).

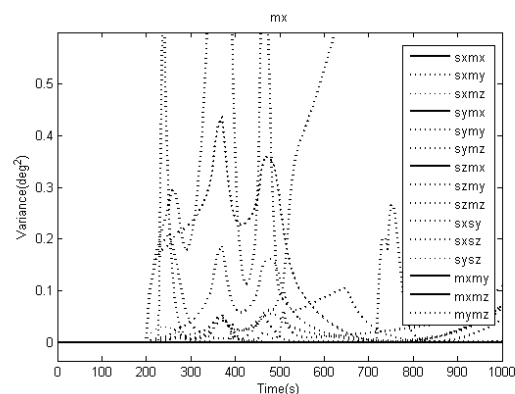
Scenario 2: fault in the x component of the magnetometer and in the y component of the sun sensor

In this scenario, A fault with the magnitude 5000 nT occurs in the m_x at time $t = 200s$. After that, at time $t = 400s$, another fault with the magnitude 0.25° is introduced in the su_y . In this case, after occurrence of the first fault, the minimum variance of the intermediate Euler angles changes significantly. Since, the first fault is not resolved and then the second fault occurs, the variance still remains above the threshold value. Because the detection

process in this scenario is similar to the first scenario, the resulted graphs are not presented here. Now, the fault isolation mechanism in step 1 should be executed. Figure 10 depicts the calculated variances in Table 3. As shown in Figure 10, between times $t = 200s$ and $t = 400s$, five variances (solid lines) have not varied. It means that in this time interval, only one component has been faced to fault. So, the value 1 is assigned to F_2 (Figure 11) at time $t = 220s$ (17 samples for fault isolation together with 3 samples for fault detection).



Slika 6. Fault detection in scenario 1 using the variation of the variance value

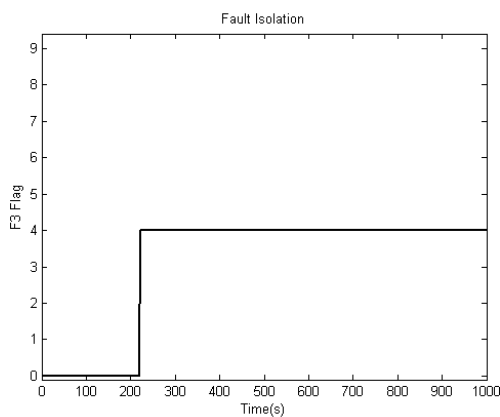
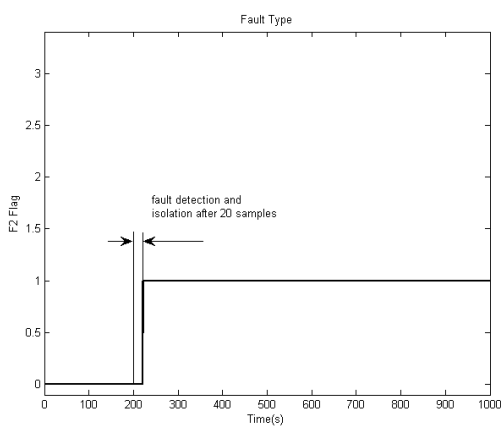


Slika 7. Two-components variances in scenario 1

In this time interval it can also be shown that the variance corresponding to m_x is minimum and so this component is faulty, as a result the value 4 is assigned to F_3 . With attention again to Figure 10, it can be observed that after time $t = 400s$, only one variance has not changed significantly (the blue solid line that is corresponding to m_x-su_y components). This means that after this time, two

components have been subjected to fault and we should evaluate step 2 in the fault isolation chart. Since, after time $t = 400s$, the variance corresponding to m_x-su_y has the minimum value (row 2 in Table 3), the value 2 is assigned to F_2 (Figure 11), also the value 4 is assigned to F_3 . Note that it takes 17 samples to isolate the new faulty condition and so F_2 and F_3 values are changed after this time interval.

Since the fault detection and isolation processes for type 3 faults (step 3 in the fault isolation chart) are similar to the scenario 2 for type 2 faults, the related results are ignored here.

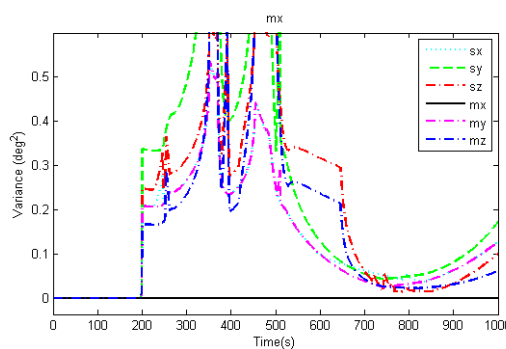


Slika 8. The values assigned to flags (a) F_2 (b) F_3 in scenario 1

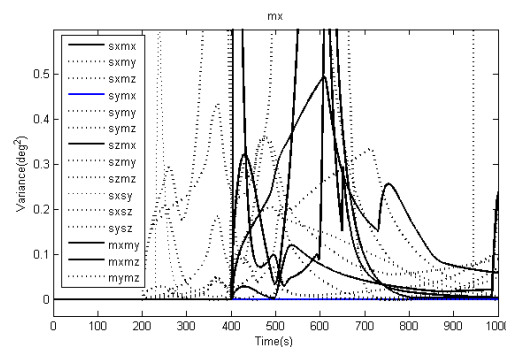
Scenario 3: fault in the x and y components of the magnetometer and in the x component of the sun sensor

A fault with the magnitude 5000nT is introduced in the m_x at time $t = 150s$. After that, another fault with the magnitude 5000 nT occurs in the m_y at time $t = 300s$. Then a fault with the magnitude 0.25° occurs in the su_x at

time $t = 500s$. In this scenario, the fault detection mechanism is performed similar to the previous scenarios. Also, the fault isolation is done similar to the previous scenario until time $t = 500s$. As shown in Figure 12, between times $t = 150s$ and $t = 300s$, 5 variances (solid lines) have changed, so fault has occurred in one component. Between times $t = 300s$ and $t = 500s$, all variances except the variance corresponding to m_x-m_y (the blue solid line) have changed significantly. After fault occurrence in three mentioned components (at time $t = 500s$), all variances (even the variance corresponding to m_x-m_y) have changed and exceeded the threshold value (the red dash line).



Slika 9. One-component variances in scenario 1

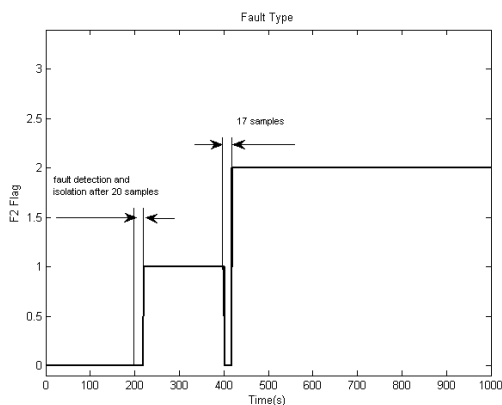


Slika 10. Two-components variances in scenario 2

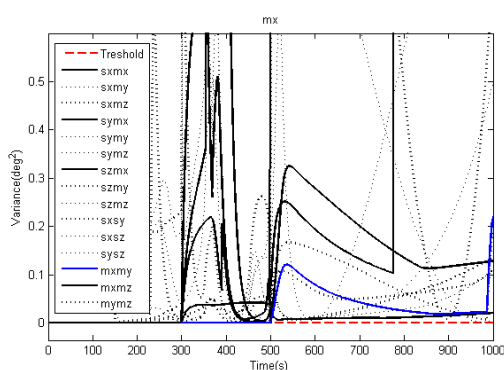
This analysis shows that after time $t = 500s$, fault does not belong to types 1, 2 and 3. Therefore, a type 4 fault is declared, i.e. more than two components are faulty. After this time, the value 0 is assigned to flags F_2 and F_3 , also at this time F_4 (Figure 13) is triggered with a 17 samples delay. Similarly, by carrying out of simulations for different scenarios, the validity of the proposed fault detection and isolation algorithms could be shown. The associated graphs are not shown here for brevity.

7 CONCLUSION

This paper described design steps of Euler angles based fault detection and isolation algorithms for a three axis satellite. Performed simulations demonstrated the proper performance of fault detection process using the derived variances. Also, using the suitable categorization of calculation methods, the fault source was isolated in four stages. The conducted simulations demonstrated that the variations profiles of variances in the mentioned stages are completely different to each other that provide the ability to distinguish the supposed fault sources. The prominent feature of the suggested methods is that can provide fault detection and isolation independent of the health status of actuators. Future work is planned to provide the accommodation feature after fault occurrence.



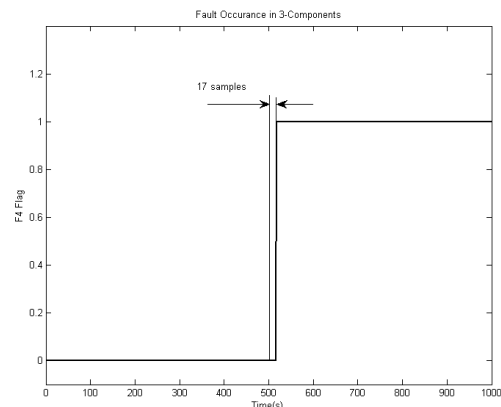
Slika 11. The values assigned to flag F2 in scenario 2



Slika 12. Two-components variances in scenario 3

Literatura

- [1] J.F. Castet and J.H. Saleh, "Satellite and satellite subsystems reliability: Statistical data analysis and modeling", *Re-*



Slika 13. The value assigned to flag F_4 after time $t = 500s$

liability Engineering and System Safety, vol. 94, pp. 1718-1728, 2009.

- [2] R. Wertz, *Spacecraft attitude determination and control*. Dordrecht, Netherlands: Kluwer academic publishers, 1978.
- [3] V. Venkatasubramanian, R. Rengaswamy and S.N. Kavuri, "A review of process fault detection and diagnosis part I: quantitative model-based methods", *Computers & Chemical Engineering*, vol. 27, pp. 293-311, 2003.
- [4] R. Iserman, *Fault Diagnosis Systems: An Introduction from Fault Detection to Fault Tolerance*, Germany, Springer, 2006.
- [5] F. N. Pirmoradi, F. Sassani and C.W.D. Silva, "Fault detection and diagnosis in a spacecraft attitude determination system", *Acta Astronautica*, vol. 65, pp. 710-729, 2009.
- [6] K. Xiong, C. W. Chan and H. Y. Zhang, "Detection of satellites attitude sensor faults using the UKF", *IEEE Transactions on Aerospace and Electronics Systems*, vol. 43, no.2, pp. 480-491, 2007.
- [7] H.E. Soken, C. Hajiyev, "Pico satellite attitude estimation via robust unscented Kalman filter in the presence of measurement faults", *ISA Transactions*, vol. 49, pp. 249-256, 2010.
- [8] J. Bae, Y. Kim, "Attitude estimation for satellite fault tolerant system using federated unscented Kalman filter", *International Journal of Aeronautical and Space Sciences*, vol. 2, no. 2, pp. 80-86, 2010.
- [9] N. Venkateswaran, M.S. Siva and P.S. Goel, "Analytical redundancy based fault detection of gyroscopes in spacecraft applications", *Acta Astronautica*, vol. 50, no. 9, pp. 535-545, 2002.
- [10] J. Li, C. W. Chan and H. Y. Zhang, "Asymptotic local approach in fault detection based on predictive filters", *Journal of Guidance, Control and Dynamics*, vol. 28, no. 6, pp. 1112-1122, 2005.

- [11] H. A. Talebi, K. Khorasani, "An intelligent sensor and actuator fault detection and isolation scheme for nonlinear systems", in *Proceedings of the 46th IEEE conference on decision and control*, (New Orleans, USA), pp. 2620-2625, Dec. 2007.
- [12] Q. Wu and M. Saif, "Robust fault diagnosis for satellite attitude systems using neural state space models", in *IEEE International Conference on Systems, Man and Cybernetics*, (Hawaii, USA), pp. 1955-1960, Oct. 2005.
- [13] R. He, X. Chen, Y. Geng and Y. Zhang, "Integrated fault detection and fault-tolerant based on sliding mode observer", in *4th IEEE Conference on Industrial Electronics and Applications*, ICIEA, (Xi'an, China), pp. 3454-3457, May 2009.
- [14] Q. Wu and M. Saif, "An overview of robust model-based fault diagnosis for satellite using sliding mode and learning approaches", in *IEEE international conference on systems, man and cybernetics, ISIC*, (Montreal, Canada), pp. 3159-3164, Oct. 2007.
- [15] L. Wu, Y. Zhang and H. Li, "Research on fault detection for satellite attitude control systems based on sliding mode observers", in *IEEE international conference on mechatronics and automation*, (Changchun, China), pp. 4408-4413, Aug. 2009.
- [16] Q. Wu and M. Saif, "Robust fault diagnosis of a satellite system using a learning strategy and second order sliding mode observer", *IEEE Systems Journal*, vol. 4, no. 1, pp. 112-121, 2010.
- [17] M. J. Sidi, *Spacecraft dynamic and control*, New York, USA: Cambridge university press, 1997.



Seyyed Saeed Nasrolahi received the B.S. and M.S. degrees in electrical engineering, control tendency, from the Iran University of Science and Technology (IUST), Iran, in 2006 and 2011 respectively. Since 2012 he has researched in Amirkabir University of Technology (Tehran Polytechnic) as a Ph.D. candidate in control engineering. His research interests are in the field of fault detection and isolation, satellite attitude control and satellite attitude determination.



017165

Hossein Bolandi received the B.S. degree in control from the Norfolk State University, USA, in 1984. He received the M.S. and Ph.D. degrees in control from the George Washington University, USA, in 1986 and 1990 respectively. Since 1991 he has been an assistant professor in the Department of Electrical Engineering at the Iran University of Science and Technology, Iran. His research areas are in the field of control and automation and robotics and his interests include adaptive control systems, satellite attitude determination and satellite attitude control and fault detection and diagnosis.

Mostafa Abedi received the B.S. degree in electrical engineering from the Shahid Chamran university, Iran, in 2004. He received the M.S. and Ph.D. degrees in automation and control from the Iran University of Science and Technology (IUST), Iran, in 2007 and 2013 respectively. Since 2008 he worked as a control expert at the IUST satellite center. His research interests are in the field of fault detection and isolation, satellite attitude control and satellite attitude determination.

AUTHORS' ADDRESSES

Seyyed Saeed Nasrolahi, M.Sc.

Assoc. Prof Hossein Bolandi, Ph.D.

Mostafa Abedi, M.Sc.

School of Electrical Engineering,

Iran University of Science and Technology,

Iran University of Science and Technology street, Hengam,

Narmak, 1684613114, Tehran, Iran

email: ss_nasrolahi@elec.iust.ac.ir, mostafa_

abedi@iust.ac.ir, h_bolandi@iust.ac.ir

Received: 2012-10-16

Accepted: 2013-04-03